Exploration of the molecular mechanism of the bone protective effect activated by Si-Wu- Tang in ApoE -/- mice fed a high-fat diet through network pharmacology analysis combined with in vivo experiments

Jiadi Yang
Beijing University of Chinese Medicine
Danning Shi
Beijing University of Chinese Medicine
Zeye Zhang
Beijing University of Chinese Medicine
Meng Zhang
Beijing University of Chinese Medicine
Qian Yan
Beijing University of Chinese Medicine
Yueshuang He
Beijing University of Chinese Medicine
Jiao Liu
Beijing University of Chinese Medicine
Piwen Zhao (pw__zhao@163.com)
Beijing University of Chinese Medicine

Research Article

Keywords: Si-Wu-Tang (SWT), phytoestrogens, PI3K/AKT, osteopenia, apolipoprotein E (ApoE -/-)

Posted Date: April 14th, 2022

DOI: https://doi.org/10.21203/rs.3.rs-1544746/v1

Abstract

Background

Bone protective effect of Si-Wu-Tang (SWT), a classical prescription of traditional Chinese medicine, is verified in clinical for thousand years. However, its mechanisms were still unclear. This study aims to investigate the molecular mechanism in ApoE -/- mice fed a high-fat diet combining network pharmacology and in-vivo experiments.

Methods

Femurs were collected from 6 ~ 8-week-old female *ApoE-/-* C57BL/6J mice (n = 12, 18–22 g) and their age-matched wild-type (WT) littermates C57BL/6J mice (n = 6, 18–20 g). They were divided into 3 groups: the control, SWT and model groups. Serum levels of high-density lipoprotein cholesterol (HDL-C) and low-density lipoprotein cholesterol (LDL-C) were measured by the serum biochemical index. HE staining and immunohistochemistry analysis were performed to observe the pathological tissue structure and the location and expression level of targets from the pathway screened out by the network pharmacology method. Western blot (WB) and RT-PCR analyses were performed to detect the expression levels of target proteins and mRNAs, respectively.

Results

The results of the network pharmacology analysis showed that the mechanism of SWT in treating osteopenia was closely related to the oestrogen receptor (ER) signalling pathway. In vivo experiments indicated that, compared with control group, the distribution of bone trabeculae was sparse, and the bone density decreased. The levels of HDL-C and LDL- C in the serum of the model group increased significantly ($p < 0.01$). The expression of GPER, PI3K, AKT and BCL-2 in the bone tissue of the model group decreased, and P53, BAX, ERα and ERβ were upregulated. Compared with the model group, the body mass of the SWT group increased slowly. The bone density and the distributions of bone trabeculae both increased. The expression of ERα, ERβ, GPER, PI3K, AKT and BCL-2 increased. The decreased expression of apoptotic genes, including P53 and BAX, was observed.

Conclusion

SWT significantly reduced bone loss in *ApoE -/-* mice fed a high-fat diet. An important mechanism might be that SWT could activate the PI3K/AKT signalling pathway mediated by ER and then inhibit apoptosis-related proteins to exert bone protective effects.

Introduction

Bone loss, also known as osteopenia, is a common complication in human solid tumours and the main risk factor for fractures in the elderly [1, 2]. In addition, after complete hysterectomy and bilateral ovariectomy (OVX), osteopenia often occurs due to oestrogen deficiency [3]. If osteopenia is not stopped early, it will develop into osteoporosis. Osteoporosis is characterized by decreased bone density and strength due to the excessive loss of bone protein and mineral content [4]. It is estimated that more than 200 million people suffer from osteoporosis worldwide, and 30% of postmenopausal women are affected by osteopenia [5]. Studies have shown that lipid metabolism has a pivotal impact on bones [6, 7]. It has been clinically observed that plasma low-density lipoprotein (LDL) is negatively correlated with the level of bone mineral density (BMD) [8].

ApoE deficiency has a considerable influence on the transport of cholesterol and can regulate the effect of a high fat load on bones [9, 10]. High-density lipoprotein (HDL) is closely related to bone physiology and pathology [8]. Studies in animal models have revealed that dysfunctional or disordered HDL can affect bone mass in many different ways [11, 12]. Specifically, reducing HDL levels is related to the development of an inflammatory microenvironment that affects the differentiation and function of osteoblasts [13]. Furthermore, increasing bone marrow obesity will also worsen the function of osteoblasts, thereby worsening bone synthesis and reducing bone formation [13]. It has been reported that a long-term high-fat diet (HFD) can enhance osteopenia and reduce the bone strength of animals[14]. In addition, *ApoE*$^{-/-}$ mice fed a HFD exhibited increased osteoblast apoptosis and increased *P53* mRNA expression in bone marrow adherent cells. This result suggested that *ApoE* gene defects can stimulate the P53-mediated apoptosis of osteoblasts and enhance the reduction of bone formation induced by HFD, thereby disrupting the balance between bone formation and bone resorption [8, 15].

The ancient Chinese medicinal literature indicates that Chinese herbal medicine has been used to strengthen bone and treat osteoporosis in China for several thousand years[16]. Si-Wu-Tang (SWT), a traditional Chinese medicine (TCM) formula, is widely used and has multiple functions, including enriching blood, anti-inflammatory and lowering blood lipids [17]. Clinically, it is mainly used to treat gynaecological diseases and other oestrogen-related diseases [17, 18]. Importantly, it has been reported to exert essential effects on relieving symptoms of osteoporosis [17, 19]. Oestrogen is a sex steroid hormone with a wide range of functions [20]. In addition to the reproductive organs, it also involves other organs and tissues, including the cardiovascular system and the exercise system [18, 19, 21]. Oestrogen mainly acts by binding to oestrogen receptors (ERs), including oestrogen receptor alpha (ERα), oestrogen receptor beta (ERβ) and the G protein-coupled oestrogen receptor (GPER, formerly known as GPR30). After binding to the ER, it can regulate gene transcription in the nucleus or activate kinases in the cytoplasm to play a broader role[20]. The oestrogen receptor is activated in an oestrogen-dependent or oestrogen-independent manner, interacts with the phosphatidylinositol 3-kinase (PI3K)/protein kinase B (AKT) cell signalling pathway in the cytoplasm and exerts vital biological effects [22].

Although SWT as a classical prescription has been used in clinical practice for a long time, its molecular mechanism still needs to be clarified due to the complex characteristics of its multi-compound and multi-target effects [23]. Network pharmacology is an innovative method based on systems biology, including

the construction of disease networks, drug target networks and drug-disease networks [24]. This method aims to uncover the complexity of biological systems, drugs and diseases, which has definite parallels to TCM [18]. In the current study, network pharmacology combined with in vivo experiments were performed to explore the molecular mechanism of the bone protective effect activated by SWT on *ApoE*$^{-/-}$ mice fed a high-fat diet. The entire work flow is illustrated in Fig. 1.

Materials And Methods

Main reagents and instruments

Primary antibodies against ERα (Immunoway, YT1634), ERβ (Santa Cruz, SC-390243), GPER (Abcam, ab260033), PI3K (67071-1-Ig), AKT (60203-2-Ig), P53 (60283-2-Ig), BAX (50599-2-Ig) and BCL-2 (60178-1-Ig), as well as the secondary antibody Anti - Rabbit IgG (H + L) (SA00001–2), Anti-Mouse IgG (H + L) (SA00001–1) were purchased from Proteintech Company (China). Total RNA Extraction Kit (G3013) and cDNA Synthesis Kit (G3331) was from Servicebio (Wuhan, China). Micro-sampler (Gilson, France), Electrophoresis instrument (Beijing Biotechnology Co., Ltd., BG-subMIDI), Cryogenic centrifuge (Sigma, Germany, 3-30K), SDS–PAGE electrophoresis system (BIO-Rad, USA), Gel imaging system (UVP, USA, GelDoc-It310), Decolouring shaker (Hamen Qilin Bell Instrument Manufacturing Company, TS-100), Super resolution microscopy imager (Lecia Aperio Versa, USA), Rt-qPCR instrument (Bio-rad, CFX, USA).

Experimental herbs

SWT was provided by Beijing Dongzhimen Hospital. Briefly, 12g Shudihuang (*Rehmannia glutinosa*), 9g Danggui (*Angelica sinensis*), 9g Baishao (*Paeonia lactiflora Pall*), 6g ChuanXiong (*Conioselinum anthriscoides*) in 1000 mL reverse osmosis water is simmered to 250 mL to obtain an extract. Then SWT was prepared by freeze-drying technology. The composition of SWT by High-performance liquid chromatography (HPLC) has been analyzed in our previous study to ensure the quality of SWT applied in the current study [25].

Experimental animals and groups

In the current study, 12 ApoE$^{-/-}$ female mice and 6 ordinary female mice of 6–8 weeks Specific Pathogen Free (SPF) C57BL/6J (18–22 g) were used, and all of them were purchased from Wei Tong Li Hua Biotechnology Co., Ltd. The laboratory animal quality certificate number was SCXK (Jing) 2016-0006. Co60 rat maintenance feed and high-fat feed (HFD, containing 1.25% cholesterol and 20% fat, special diet order, D12079B) were purchased from Beijing Hua Fu Kang Biotechnology Co., Ltd. The laboratory animal-feed quality certificate number was SCXK (Beijing) 2019-0008. The experimental animals were kept in a constant temperature control room (25°C), circulated in light and dark for 12 hours, and had free access to feed and water. After 7 days of adaptive feeding, they were randomly divided into 3 groups: the model group (*ApoE*$^{-/-}$), SWT (*ApoE*$^{-/-}$) group and control group (WT). WT mice were fed ordinary maintenance feed, and *ApoE*$^{-/-}$ mice were fed high-fat feed for 8 weeks. After 8 weeks, the mice in the model group and control group were given ddH2O, and the SWT group was given Si-Wu-Tang. Then, after

four weeks of gavage, the femurs of the mice were collected, as shown in Table 1. After the blood was taken, the left femur was quickly separated from the mice, and fresh tissue was frozen in liquid nitrogen for Western blot analysis. Part of the tissue was fixed in 4% paraformaldehyde, and the remaining tissue was used to make paraffin sections and frozen sections. The ethics approval number for the use of animals in this study was BUCM-4-2021121501-4098.

Table 1
Experimental animal grouping

	Mouse strain	number	feed	Gavage solution
Control	C57BL/6J	6	Standard diet	ddH_2O
Model	*Apoe*$^{-/-}$ C57BL/6J	6	HFD	ddH_2O
SWT	*Apoe*$^{-/-}$ C57BL/6J	6	HFD	SWT

Body weight and serum lipid levels

Serum samples were placed in an ice-water bath. The sample to be tested and working reagents were separately prepared and mixed according to the requirements of the kit using the double reagent method. Corresponding parameters were set on the automatic biochemical analyser. Then, the values of high-density lipoprotein cholesterol (HDL-C) and low-density lipoprotein cholesterol (LDL-C) were measured on an automatic biochemical analyser. Finally, the experimental results were exported and analysed.

Network Pharmacology

SWT is composed of four herbs: Danggui (*Angelica sinensis*), Shudihuang (*Rehmannia glutinosa*), Baishao (*Paeonia lactiflora Pall*) and Chuanxiong *(Conioselinum anthriscoides*) [18]. First, the active components of SWT were screened through the Chinese Medicine Pharmacology Database and Analysis Platform (TCMSP http://lsp.nwu.edu.cn/tcmsp.php). The selection criteria were oral bioavailability (OB) ≥ 30% and drug-likeness (DL) ≥ 0.18. Then, the target information of the active components was collected. The targets of the two databases as drug target data were integrated for use. The SwissTarget database (http://www. Use Swiss target prediction. Ch/) were used to find targets that matched the chemical structure of the ingredients. The Online Mendelian Inheritance in Man (OMIM: http://www.omim.org/) and Gene Cards databases (https://www.genecards.org/) were used to select targets related to “osteopenia”. A Venn diagram online tool (http://bioinformatics.psb.ugent.be/webtools/Venn/) was used to integrate the corresponding target of SWT and the target of osteopenia to obtain the overlapping targets of drug-disease. The previously obtained disease-drug common targets were imported into the String database (https://string-db.org/) to obtain a protein interaction (PPI) map, and Cytoscape 3.6.1 was used for visualization. The top 30 targets were connected as key targets. Then, the Cluster Profiler software package in R software was used for Gene Ontology (GO) and Kyoto Encyclopaedia of Genes and Genomes (KEGG) pathway enrichment

analysis on disease-drug target genes to obtain related functions and pathways. The screening criterion was FDR < 0.05. According to the number of genes and p value in the pathway enrichment results, combined with relevant literature analysis, the key pathways and targets related to SWT on osteopenia were obtained.

Haematoxylin-eosin staining

The femurs of mice were decalcified and embedded in paraffin. Then, they were sectioned (5 μm thick). The sections were dewaxed in xylene, decolorized in ethanol, stained with haematoxylin, differentiated in acetic acid, washed, stained with eosin, dehydrated, and mounted. Finally, the staining was observed under a microscope.

Western blot analysis

After weighing and grinding the femur tissue, 1 ml lysate per 100 mg bone tissue was added to fully lyse it on ice for 30 min, centrifuged for 15 min (4℃, 12000 r/min), and the supernatant was used. The protein concentration was measured with a BCA kit, and the protein was denatured with 5x buffer. After SDS–PAGE electrophoresis, to the PVDF transfer membrane, 5% skimmed milk powder was added, and it was sealed at room temperature for 1.5 hours; the PVDF membrane was then incubated in ERα, ERβ, GPER, PI3K, AKT, P53, BAX, BCL-2, β-actin primary antibody incubation solution at 4°C overnight; then it was incubated in the corresponding secondary antibody at room temperature for 1 h. The luminescent fluid was configured according to the ultrasensitive ECL colour development kit, and images were obtained on a gel imager. ImageJ software was used to analyse the grey value of each group of bands, and β-actin was used as the internal reference to calculate the expression of each protein.

Immunochemistry

Paraffin sections are deparaffinized and washed 3 times with PBS for 3 min; the tissue specimens are soaked in 0.01% TritonX-100 for 15 min to permeate the membrane, washed with PBS buffer for 3 min × 3 times; the sections were placed in sodium citrate antigen retrieval solution and then placed in a microwave oven (medium-high for 3 min and medium-low for 15 min); after natural cooling, it was washed with PBS buffer for 3 min × 3 times; the endogenous peroxidase blocker was dropped on the tissue section, and then it was washed with PBS buffer for 3 min × 3 times; the goat serum working solution was dripped in for blocking, and then it was stewed for 20 min; the primary antibody was incubated, and the section was placed in a humid box overnight at 4℃; the secondary antibody was then incubated: an appropriate amount of reaction enhancement solution was added, and it was then incubated at room temperature for 20 min, washed with PBS buffer for 3 min × 3 times and dropped again. Enhanced enzyme-labelled goat anti-rabbit/mouse IgG polymer was added; it was then incubated at room temperature for 20 minutes and washed with PBS buffer 3 times for 3 minutes. For DAB staining, the prepared DAB staining solution was added dropwise to the section, and then incubated in the dark for 10 minutes, and the staining conditions were observed under a microscope. Next it was rinsed with tap water, counterstained with haematoxylin by add haematoxylin for 1 min and rinsing with tap water; then the dehydration of the section was performed; after air-drying, neutral gum was added, and it was covered

with a cover glass; the section was scanned with a super resolution microscopy imager, and ImageJ was used to perform image analysis.

Quantitative RT–PCR

After grinding the mouse femur tissue with liquid nitrogen, the total RNA of the sample was extracted according to the TRIzol method. The RNA concentration and purity were determined using a nucleic acid concentration analyser, and then cDNA was synthesized using Invitrogen reverse transcription kit superscript III. PCR tubes were used to equip the reverse transcription products; each prepared three tubes for use: 2 × qPCR Mix 7.5μl 2.5Mm gene primer 1.5 μl reverse transcription product 2.0 μl ddH2O 4.0μl; PCR amplification conditions: pre-denaturation 95℃, 10 min cycle (40 times) 95℃, 15 s → 60 ℃, 30 s; melting curve: 65℃ → 95 ℃, heating up 0.3 ℃ every 15 s. Using β-actin as the internal reference, the relative expression of each target was calculated by the $2^{-\Delta\Delta Ct}$ method. The primers used for RT-qPCR in the current study was listed in Table 2. The results were processed using the $2^{-\Delta\Delta Ct}$ method and finally processed with GraphPad Prism 8.0.

Table 2
The mRNA sequences of the targets obtained from network analysis.

Gene name	Forward primer	Reverse primer
ERα	GAAGGCTGCAAGGCTTTCTTTA	AAGGCAGGGCTATTCTTCTTAGTG
ERβ	TGATGATGTCCCTCACGAAGC	AGAACGAGGTCTGGAGCAAAG
GPER	AGTCTTTCCGTCACGCCTACC	GGCTCGTCTTCTGCTCCACA
PI3K	CAAACCACCCAAGCCCACTA	AGGTCCCATCAGCAGTGTCTC
AKT	CTTTATTGGCTACAAGGAACGGC	TGGGTGAGCCTGATCGGAA
P53	CCCTCTGAGCCAGGAGACATT	CCCAGGTGGAAGCCATAGTTG
BCL-2	GCTACCGTCGTGACTTCGCA	CATCCCAGCCTCCGTTATCC
BAX	CCGGCGAATTGGAGATGAAC	AAGTAGAAGAGGGCAACCACGC

Statistical analysis

This experiment uses SPSS 20.0 software for data processing. The data conforming to the normal distribution or approximately conforming to the normal distribution are expressed as the mean ± standard deviation ($\bar{x}$ ± s). If the variance was homogeneous, the comparison between multiple groups was performed by one-way analysis of variance, and the pairwise comparison between groups was performed by the LSD-test. The correlation between each group was tested by Pearson's test. The difference was statistically significant at $P < 0.05$.

Results

SWT quality inspection

To ensure the quality of SWT applied in the current study, compositions of SWT were analyzed by HPLC technique. Seven chemical components of SWT indicated in the Pharmacopoeia of the People's Republic of China were selected as indicators, including chlorogenic acid, caffeic acid, paeoniflorin, ferulic acid, acteoside and senkyunolide A. The compositions of SWT freeze-dried powder were exhibited in **Supplementary Table 1** and **supplementary Fig. 1**.

The body weight and the serum biochemical index in mice

The body weights of the experimental mice shown in Table 3 suggested that compared with the control group, the SWT and model groups were heavier ($p < 0.05$). And then, after 4 weeks gavage, SWT group was lighter than model group. The serum biochemical index shown in Table 4 indicated that compared with the control group, the levels of HDL-C and LDL-C in the serum of the model group increased significantly.

Table 3
Body weight of experimental animals

Groups	n	8 weeks	12 weeks
Control	6	22.16 ± 0.38	21.30 ± 0.38
Model	6	23.98 ± 1.08*	24.92 ± 0.85**
SWT	6	24.50 ± 0.72**	22.88 ± 1.11
(Compared with control group, *$p < 0.05$, **$p < 0.01$)			

Table 4
Blood lipid related indexes in the serum of experimental animals ($\bar{x} \pm s$)

Group	n	HDL-C (mmol/L)	LDL-C (mmol/L)
Control	6	1.08 ± 0.06	0.41 ± 0.02
Model	6	2.26 ± 0.21	18.34 ± 0.45

Oestrogen receptor signalling pathway screened from network pharmacology analysis

According to the retrieved results of the TCMSP database, the effective blood components of SWT were obtained, as shown in Fig. 2A. The active ingredients were filtered to identify the corresponding related targets. OMIM and GeneCards databases were used to select key targets related to “osteopenia”. Through

the integration of the Venn diagram online tool, 63 drug-disease targets were obtained, including BCL-2 and BAX, as shown in Fig. 2B. The STRING database was used to obtain the protein interaction diagram, as shown in Fig. 3. GO analysis in FunRich was performed to further investigate the biological functions of 63 SWT-osteopenia targets. The results indicated that these targets primarily existed in cytosol, membrane raft, receptor complex and mitochondrial outer membrane and other regions of the cell and were involved in toxic substance, lipopolysaccharide, cellular response to lipid and other biological processes (Fig. 4A-B). Moreover, nuclear receptor activity, cysteine-type endopeptidase activity involved in apoptotic signaling pathway, protein kinase activity and protein phosphatase binding are the principal molecular functions of SWT against osteopenia (Fig. 4C). To further reveal the potential mechanism of the anticancer effect of SWT on osteopenia, Kyoto Encyclopedia of Genes and Genomes (KEGG) pathway enrichment analysis was conducted on the 63 targets by the ClusterProfiler package. According to the count value and p value, the first 20 channels were selected (Fig. 4D), of which the key pathways were pathway in cancer, Oestrogen signalling pathway, MAPK signalling pathway and regulation of lipolysis in adipocytes. In conclusion, the effect of SWT on osteopenia have a close association with cellular response to lipid, protein kinase and protein phosphatase binding on lipid metabolism and apoptosis, especially in the receptor complex and mitochondrial outer membrane. Combined with literature search, the results of GO and KEGG indicated that the relevant pathway to this study was the oestrogen receptor signalling pathway. To explore the multitarget pharmacological mechanism of the bone protection of SWT, we detected targets of the ER pathway, including ERα, ERβ, GPER, PI3K, AKT, P53, BCL-2 and BAX.

Observation of the pathological tissue morphology of mice

As shown in Fig. 5, the SWT group meliorated the pathological morphology of the bone tissue of the model mice. HE staining found that the trabecular bones of the control group were evenly distributed and arranged in an orderly manner, with small intervals between the trabecular bones. The trabecular bones of the model group were sparsely distributed, with scattered arrangements and broken points. Compared with the model group, the SWT group meliorated the distribution and arrangement of bone trabeculae in *ApoE*$^{-/-}$ mice fed a high-fat diet.

The protein expression of ERα, ERβ, GPER, PI3K, AKT, P53, BCL-2 and BAX in mice.

Western blot results showed that compared with the control group, the expression of classic oestrogen receptors, including ERα, ERβ and GPER, in the SWT group, as well as the expression of PI3K, AKT and BCL-2 proteins, were significantly increased, while the expression of apoptosis genes, including P53 and BAX, was significantly decreased ($P < 0.01$). Compared with the control group, the expression of GPER, PI3K, AKT and BCL-2 protein in the bone tissue of the model group was downregulated. P53, BAX, ERα and ERβ were upregulated. When Si-Wu-Tang exerts an oestrogen-like effect on bone tissue, the effect of regulating GPER is more obvious (Fig. 6).

The expression position and expression level of ERα, ERβ, GPER, PI3K, AKT, P53, BCL-2 and BAX in mice.

As shown in Fig. 7, the results of femoral immunohistochemistry show that the expression of each target in bone tissue is mainly located in bone cells and osteoblasts, so we zoomed in to observe the specific location of each target in the cell. Positive bone cells and osteoblasts stained brown–yellow particles. It can be seen from the Fig. 7 that P53, BAX and BCL-2 are mainly distributed in the cell cytoplasm; ERα and ERβ are distributed in the nucleus, and GPER is distributed on the cell membrane, and PI3K and AKT are both distributed on the cell membrane and nucleus. Compared with the model group, SWT increased the expression of ERα, ERβ, GPER, PI3K, AKT and BCL-2 in the femur and decreased the expression of P53 and BAX, which was approximately the same trend as the results of WB.

The mRNA expression of ERα, ERβ, GPER, PI3K, AKT, P53, BCL-2 and BAX in mice.

The RT–PCR results were showed in Fig. 8, compared with the control group, the mRNA expression of ERα, ERβ, P53 and BAX in the model group was relatively increased. The expression of GPER, PI3K, AKT and BCL-2 was significantly decreased ($P < 0.01$). Compared with the control group, the expression of ERα, ERβ, GPER, PI3K, AKT and BCL-2 in the SWT group increased significantly, and the expression of P53 and BAX decreased significantly. The expression levels of WB and mRNA were roughly the same. The results showed that when SWT exerted an effect on bone tissue, the regulation of different oestrogen receptors was different, and the regulatory effect on GPER was more obvious (Fig. 9).

Discussion

Bone is a complex tissue composed of multiple cell types that are constantly being renewed and repaired[26]. Dysregulation of bone resorption and bone formation could lead to osteopenia [27]. Accumulating studies suggest that excessive fat mass is detrimental to bone formation[9, 28, 29]. In addition, an experiment using a diet-induced obesity mouse model showed that after feeding mice a high-fat diet (HFD, 45% of energy as fat) for 14 weeks, although the body weight and bone formation markers in the cultured bone marrow mesenchymal stem cells (BMSCs) increased significantly, the volume and the number of bone trabeculae in the proximal tibia decreased [30]. Furthermore, some in vitro studies have shown that oxidized LDL inhibits the differentiation of osteoprogenitor cells into osteoblasts, and a HFD leads to atherosclerosis and reduces bone mineralization in mice[31–33]. Consistent with previous studies, the current research significantly indicated a positive relationship between serum levels of HDL-C and LDL-C and osteopenia. This result suggested that the regulation of lipid metabolism might be a potential method to inhibit the development of osteopenia.

SWT is a commonly used gynaecological clinical basic prescription[17]. Recent studies have found that SWT has a phytoestrogen effect and plays a vital role in relieving osteopenia[17, 18]. However, the potential molecular mechanism remains to be further clarified. Herein, to further detect the mechanism of SWT on osteopenia, network pharmacology combined with in vivo experiments was applied to further explore the bone protection of SWT in *ApoE*$^{-/-}$ mice fed a HFD. In this study, GO and KEGG enrichment analyses were performed to obtain the most relevant pathways—the oestrogen receptor signalling pathway - and to target ERα, ERβ, GPER, PI3K, AKT, P53, BCL-2 and BAX, as shown in Fig. 9. These results

suggested that the bone protective effect activated by SWT could be realized through the regulation of oestrogen receptor signal transduction and the PI3K/AKT pathway, and importantly, apoptosis-related mechanisms were involved.

Commonly, oestrogens exert their actions by binding with oestrogen receptors (ERs)[34]. ERα and ERβ act as transcription factors mediating genomic effects[35]. In addition, GPER was recently described as a seven-transmembrane receptor that mediates nongenomic oestrogenic signalling[36]. These pathways include calcium mobilization, apoptosis signalling pathway, transactivation of epidermal growth factor receptor (EGFR), and the subsequent activation of PI3K/AKT signalling pathways[37, 38]. Currently, it has been reported that SWT could promote the proliferation of osteoblasts and increase the expression levels of the downstream signalling molecules PI3K and p-AKT mediated by GPER[39]. In this study, the increased expression of receptor proteins, including ERα, ERβ and GPER in the SWT group, indicated that SWT could exert bone protective effects through the oestrogen receptor signalling pathway. The PI3K/AKT signalling pathway has been reported to play an essential role in bone formation, involving the regulation of a wide variety of cellular processes, mainly including the proliferation of osteoblasts. In the current study, we observed the upregulation of channel proteins, including PI3K and AKT after treatment with SWT. This result suggested that the potential mechanism of bone protection under a high-fat state exerted by SWT might occur through the regulation of the PI3K/AKT signalling pathway. Recently, growing evidence has indicated that PI3K and its downstream effectors, especially AKT, are involved in the regulation of bone growth and bone formation[40]. Moreover, activated AKT suppresses MDM2 by phosphorylation, which results in the release of p53. Next, activated p53 ultimately leads to cell death[41]. A recent study demonstrated that p53-induced cell death contributed to the suppression of osteoclast genesis [2]. P53, BAX and BCL-2 are the downstream apoptin of the PI3K/AKT signalling pathway[38]. The p53 gene is a tumour suppressor gene located on the short arm of chromosome 17, named after its protein product with a molecular weight of 53[42]. Its biological function is to cause cell cycle arrest, induce apoptosis and promote differentiation[43]. It has been proved that the ApoE gene enhances the reduction in bone formation induced by a HFD through the stimulation of p53-mediated apoptosis in osteoblastic cells. In this study, the results showed that p53 protein expression in the model group was obviously increased. In addition, the expression of p53 in the SWT group was decreased. In the process of cell apoptosis, the BCL-2 gene family encodes a large number of proteins, including BCL-2 and BAX[44]. It has been demonstrated that BCL-2 overexpression in osteoblasts increases osteoblast proliferation and fails to reduce osteoblast apoptosis[45]. BAX is a proapoptotic protein that causes permeabilization of the mitochondrial membrane, freeing proapoptotic factors and mediating cellular death[31, 46]. However, the expression of BCL-2 protein can prevent cell death[47]. The current results indicated that the expression of BCL-2 in the model group was significantly downregulated and that the expression of BAX was upregulated; however, the expression of BCL-2 in the SWT group was upregulated. This result suggested that bone cell apoptosis in the model group was increased, but that in the SWT group, it was decreased. Thus, the current study revealed that the bone protective effect exerted by SWT could be recognized as the regulation of apoptosis through the PI3K/AKT signalling pathway mediated by ER.

Conclusion

In summary, our current research shows that SWT extract can meliorated the osteopenia of *ApoE*$^{-/-}$ mice fed a HFD through the ER-mediated PI3K/AKT signalling pathway, reducing the expression of P53 and BAX and promoting bone formation. It provides a certain experimental basis for clinical bone loss caused by a high-fat diet.

Declarations

Authors contribution

JD.Y designed and performed the experiment and wrote papers, DN. S processed the data and revised the manuscript, ZY. Z helped organize the thoughts, Q.Y. and YS. H performed the experiment, and J.L. edited the article, PW.Z. supervised this subject.

Finaicial support

This research was funded by the National Nature Science Foundation of China, grant number 81673764. Beijing University of Traditional Chinese Medicine School Research Project 2017 (2017-JYB-JS-175).

Declaration of Competing Interests

The authors declare that they have no known competing financial interests or personal relationships that could have appeared to influence the work reported in this paper.

Data availability

All of the information are supplied as supplementary file.

Acknowledgments

The authors would like to thank School of Life Sciences, Beijing University of Chinese Medicine, China for providing laboratory facilities.

References

1. Zhao Y, Xu Y, Zheng H, Lin N. QingYan formula extracts protect against postmenopausal osteoporosis in ovariectomized rat model via active ER-dependent MEK/ERK and PI3K/Akt signal pathways. J Ethnopharmacol. 2021;268:113644. Epub 2020/12/03. doi: 10.1016/j.jep.2020.113644. PubMed PMID: 33264660.
2. Cui J, Li X, Wang S, Su Y, Chen X, Cao L, et al. Triptolide prevents bone loss via suppressing osteoclastogenesis through inhibiting PI3K-AKT-NFATc1 pathway. J Cell Mol Med.

2020;24(11):6149–61. Epub 2020/04/30. doi: 10.1111/jcmm.15229. PubMed PMID: 32347017; PubMed Central PMCID: PMCPMC7294126.

3. Miao Q, Li JG, Miao S, Hu N, Zhang J, Zhang S, et al. The bone-protective effect of genistein in the animal model of bilateral ovariectomy: roles of phytoestrogens and PTH/PTHR1 against post-menopausal osteoporosis. Int J Mol Sci. 2012;13(1):56–70. Epub 2012/02/09. doi: 10.3390/ijms13010056. PubMed PMID: 22312238; PubMed Central PMCID: PMCPMC3269672.
4. Huang MZ, Zhuang Y, Ning X, Zhang H, Shen ZM, Shang XW. Artesunate inhibits osteoclastogenesis through the miR-503/RANK axis. Biosci Rep. 2020;40(7). Epub 2020/06/17. doi: 10.1042/BSR20194387. PubMed PMID: 32542308; PubMed Central PMCID: PMCPMC7374274.
5. Barrios-Moyano A, De la Peña-García C. [Prevalence of osteoporosis and osteopenia in patients occupationally active]. Acta ortopedica mexicana. 2018;32(3):131–3. Epub 2018/12/07. PubMed PMID: 30521703.
6. Sabry M, Mostafa S, Rashed L, Abdelgwad M, Kamar S, Estaphan S. Matrix metalloproteinase 9 a potential major player connecting atherosclerosis and osteoporosis in high fat diet fed rats. PLoS One. 2021;16(2):e0244650. Epub 2021/02/12. doi: 10.1371/journal.pone.0244650. PubMed PMID: 33571214; PubMed Central PMCID: PMCPMC7877768.
7. Wu X, Ma Y, Su N, Shen J, Zhang H, Wang H. Lysophosphatidic acid: Its role in bone cell biology and potential for use in bone regeneration. Prostaglandins & other lipid mediators. 2019;143:106335. Epub 2019/05/06. doi: 10.1016/j.prostaglandins.2019.106335. PubMed PMID: 31054330.
8. Hirasawa H, Tanaka S, Sakai A, Tsutsui M, Shimokawa H, Miyata H, et al. ApoE gene deficiency enhances the reduction of bone formation induced by a high-fat diet through the stimulation of p53-mediated apoptosis in osteoblastic cells. J Bone Miner Res. 2007;22(7):1020–30. Epub 2007/03/29. doi: 10.1359/jbmr.070330. PubMed PMID: 17388726.
9. Zhao LJ, Jiang H, Papasian CJ, Maulik D, Drees B, Hamilton J, et al. Correlation of obesity and osteoporosis: effect of fat mass on the determination of osteoporosis. J Bone Miner Res. 2008;23(1):17–29. Epub 2007/09/06. doi: 10.1359/jbmr.070813. PubMed PMID: 17784844; PubMed Central PMCID: PMCPMC2663586.
10. Mahley RW. Central Nervous System Lipoproteins: ApoE and Regulation of Cholesterol Metabolism. Arteriosclerosis, thrombosis, and vascular biology. 2016;36(7):1305-15. Epub 2016/05/14. doi: 10.1161/atvbaha.116.307023. PubMed PMID: 27174096; PubMed Central PMCID: PMCPMC4942259.
11. Parhami F, Jackson SM, Tintut Y, Le V, Balucan JP, Territo M, et al. Atherogenic diet and minimally oxidized low density lipoprotein inhibit osteogenic and promote adipogenic differentiation of marrow stromal cells. J Bone Miner Res. 1999;14(12):2067–78. Epub 2000/01/05. doi: 10.1359/jbmr.1999.14.12.2067. PubMed PMID: 10620066.
12. Tintut Y, Demer LL. Effects of bioactive lipids and lipoproteins on bone. Trends in endocrinology and metabolism: TEM. 2014;25(2):53 – 9. Epub 2013/11/05. doi: 10.1016/j.tem.2013.10.001. PubMed PMID: 24183940; PubMed Central PMCID: PMCPMC3946677.

13. Papachristou NI, Blair HC, Kypreos KE, Papachristou DJ. High-density lipoprotein (HDL) metabolism and bone mass. The Journal of endocrinology. 2017;233(2):R95-r107. Epub 2017/03/21. doi: 10.1530/joe-16-0657. PubMed PMID: 28314771; PubMed Central PMCID: PMCPMC5598779.
14. Wohl GR, Loehrke L, Watkins BA, Zernicke RF. Effects of high-fat diet on mature bone mineral content, structure, and mechanical properties. Calcified tissue international. 1998;63(1):74–9. Epub 1998/06/26. doi: 10.1007/s002239900492. PubMed PMID: 9632850.
15. Saglar E, Yucel D, Bozkurt B, Ozgul RK, Irkec M, Ogus A. Association of polymorphisms in APOE, p53, and p21 with primary open-angle glaucoma in Turkish patients. Molecular vision. 2009;15:1270–6. Epub 2009/07/07. PubMed PMID: 19578553; PubMed Central PMCID: PMCPMC2704913.
16. Liu RH, Kang X, Xu LP, Nian HL, Yang XW, Shi HT, et al. Effects of the combined extracts of Herba Epimedii and Fructus Ligustri Lucidi on bone mineral content and bone turnover in osteoporotic rats. BMC complementary and alternative medicine. 2015;15:112. Epub 2015/04/19. doi: 10.1186/s12906-015-0641-4. PubMed PMID: 25889254; PubMed Central PMCID: PMCPMC4411652.
17. Wu CM, Chen PC, Li TM, Fong YC, Tang CH. Si-Wu-tang extract stimulates bone formation through PI3K/Akt/NF-κB signaling pathways in osteoblasts. BMC complementary and alternative medicine. 2013;13:277. Epub 2013/10/26. doi: 10.1186/1472-6882-13-277. PubMed PMID: 24156308; PubMed Central PMCID: PMCPMC4015792.
18. Zhang Z, Liu J, Liu Y, Shi D, He Y, Zhao P. Virtual screening of the multi-gene regulatory molecular mechanism of Si-Wu-tang against non-triple-negative breast cancer based on network pharmacology combined with experimental validation. J Ethnopharmacol. 2021;269:113696. Epub 2020/12/29. doi: 10.1016/j.jep.2020.113696. PubMed PMID: 33358854.
19. Li TM, Huang HC, Su CM, Ho TY, Wu CM, Chen WC, et al. Cistanche deserticola extract increases bone formation in osteoblasts. The Journal of pharmacy and pharmacology. 2012;64(6):897–907. Epub 2012/05/11. doi: 10.1111/j.2042-7158.2012.01483.x. PubMed PMID: 22571269.
20. Krishnan V, Heath H, Bryant HU. Mechanism of action of estrogens and selective estrogen receptor modulators. Vitamins and hormones. 2000;60:123–47. Epub 2000/10/19. doi: 10.1016/s0083-6729(00)60018-3. PubMed PMID: 11037623.
21. Ikeda K, Horie-Inoue K, Inoue S. Functions of estrogen and estrogen receptor signaling on skeletal muscle. J Steroid Biochem Mol Biol. 2019;191:105375. Epub 2019/05/09. doi: 10.1016/j.jsbmb.2019.105375. PubMed PMID: 31067490.
22. Saha T, Makar S, Swetha R, Gutti G, Singh SK. Estrogen signaling: An emanating therapeutic target for breast cancer treatment. Eur J Med Chem. 2019;177:116 – 43. Epub 2019/05/28. doi: 10.1016/j.ejmech.2019.05.023. PubMed PMID: 31129450.
23. Guo Y, Jiang Q, Gui D, Wang N. Chinese Herbal Formulas Si-Wu-Tang and Er-Miao-San Synergistically Ameliorated Hyperuricemia and Renal Impairment in Rats Induced by Adenine and Potassium Oxonate. Cellular physiology and biochemistry: international journal of experimental cellular physiology, biochemistry, and pharmacology. 2015;37(4):1491 – 502. Epub 2015/10/29. doi: 10.1159/000438517. PubMed PMID: 26509423.

24. Luo TT, Lu Y, Yan SK, Xiao X, Rong XL, Guo J. Network Pharmacology in Research of Chinese Medicine Formula: Methodology, Application and Prospective. Chin J Integr Med. 2020;26(1):72–80. Epub 2019/04/04. doi: 10.1007/s11655-019-3064-0. PubMed PMID: 30941682.
25. Zhang Z, Liu J, Liu Y, Shi D, He Y, Zhao P. Virtual screening of the multi-gene regulatory molecular mechanism of Si-Wu-tang against non-triple-negative breast cancer based on network pharmacology combined with experimental validation. J Ethnopharmacol. 2021;269:113696. doi: 10.1016/j.jep.2020.113696. PubMed PMID: 33358854.
26. Oftadeh R, Perez-Viloria M, Villa-Camacho JC, Vaziri A, Nazarian A. Biomechanics and mechanobiology of trabecular bone: a review. Journal of biomechanical engineering. 2015;137(1):0108021–01080215. Epub 2014/11/21. doi: 10.1115/1.4029176. PubMed PMID: 25412137; PubMed Central PMCID: PMCPMC5101038.
27. Rachner TD, Khosla S, Hofbauer LC. Osteoporosis: now and the future. The Lancet. 2011;377(9773):1276–87. doi: 10.1016/s0140-6736(10)62349-5.
28. Tian L, Yu X. Fat, Sugar, and Bone Health: A Complex Relationship. Nutrients. 2017;9(5). Epub 2017/05/18. doi: 10.3390/nu9050506. PubMed PMID: 28513571; PubMed Central PMCID: PMCPMC5452236.
29. Gkastaris K, Goulis DG, Potoupnis M, Anastasilakis AD, Kapetanos G. Obesity, osteoporosis and bone metabolism. Journal of musculoskeletal & neuronal interactions. 2020;20(3):372–81. Epub 2020/09/04. PubMed PMID: 32877973; PubMed Central PMCID: PMCPMC7493444.
30. Cao JJ, Gregoire BR, Gao H. High-fat diet decreases cancellous bone mass but has no effect on cortical bone mass in the tibia in mice. Bone. 2009;44(6):1097–104. Epub 2009/03/07. doi: 10.1016/j.bone.2009.02.017. PubMed PMID: 19264159.
31. Verborgt O, Tatton NA, Majeska RJ, Schaffler MB. Spatial distribution of Bax and Bcl-2 in osteocytes after bone fatigue: complementary roles in bone remodeling regulation? J Bone Miner Res. 2002;17(5):907–14. Epub 2002/05/15. doi: 10.1359/jbmr.2002.17.5.907. PubMed PMID: 12009022.
32. Zhang Q, Zhou J, Wang Q, Lu C, Xu Y, Cao H, et al. Association Between Bone Mineral Density and Lipid Profile in Chinese Women. Clinical interventions in aging. 2020;15:1649–64. Epub 2020/09/29. doi: 10.2147/cia.S266722. PubMed PMID: 32982199; PubMed Central PMCID: PMCPMC7501971.
33. Chen X, Wang C, Zhang K, Xie Y, Ji X, Huang H, et al. Reduced femoral bone mass in both diet-induced and genetic hyperlipidemia mice. Bone. 2016;93:104 – 12. Epub 2016/10/25. doi: 10.1016/j.bone.2016.09.016. PubMed PMID: 27669658.
34. Yip CH, Rhodes A. Estrogen and progesterone receptors in breast cancer. Future oncology (London, England). 2014;10(14):2293–301. Epub 2014/12/05. doi: 10.2217/fon.14.110. PubMed PMID: 25471040.
35. Fuentes N, Silveyra P. Estrogen receptor signaling mechanisms. Adv Protein Chem Struct Biol. 2019;116:135–70. Epub 2019/05/01. doi: 10.1016/bs.apcsb.2019.01.001. PubMed PMID: 31036290; PubMed Central PMCID: PMCPMC6533072.

36. Sharma G, Prossnitz ER. G-Protein-Coupled Estrogen Receptor (GPER) and Sex-Specific Metabolic Homeostasis. Advances in experimental medicine and biology. 2017;1043:427 – 53. Epub 2017/12/11. doi: 10.1007/978-3-319-70178-3_20. PubMed PMID: 29224106; PubMed Central PMCID: PMCPMC6656363.
37. Schultze SM, Hemmings BA, Niessen M, Tschopp O. PI3K/AKT, MAPK and AMPK signalling: protein kinases in glucose homeostasis. Expert reviews in molecular medicine. 2012;14:e1. Epub 2012/01/12. doi: 10.1017/s1462399411002109. PubMed PMID: 22233681.
38. Rozeboom B, Dey N, De P. ER + metastatic breast cancer: past, present, and a prescription for an apoptosis-targeted future. American journal of cancer research. 2019;9(12):2821–31. Epub 2020/01/09. PubMed PMID: 31911865; PubMed Central PMCID: PMCPMC6943351.
39. Kang WB, Cong Y, Ru JY, Ying SQ, Zhu T, Wang DS, et al. Osteoprotective effect of combination therapy of low-dose oestradiol with G15, a specific antagonist of GPR30/GPER in ovariectomy-induced osteoporotic rats. Biosci Rep. 2015;35(4). Epub 2015/07/17. doi: 10.1042/BSR20150146. PubMed PMID: 26181370; PubMed Central PMCID: PMCPMC4613688.
40. Gu Y-X, Du J, Si M-S, Mo J-J, Qiao S-C, Lai H-C. The roles of PI3K/Akt signaling pathway in regulating MC3T3-E1 preosteoblast proliferation and differentiation on SLA and SLActive titanium surfaces. Journal of Biomedical Materials Research Part A. 2013;101A(3):748–54. doi: 10.1002/jbm.a.34377.
41. Baldelli S, Ciriolo MR. Altered S-nitrosylation of p53 is responsible for impaired antioxidant response in skeletal muscle during aging. Aging. 2016;8(12):3450–67. Epub 2016/12/28. doi: 10.18632/aging.101139. PubMed PMID: 28025407; PubMed Central PMCID: PMCPMC5270679.
42. Hou Y, Hou L, Liang Y, Zhang Q, Hong X, Wang Y, et al. The p53-inducible CLDN7 regulates colorectal tumorigenesis and has prognostic significance. Neoplasia. 2020;22(11):590–603. Epub 2020/09/30. doi: 10.1016/j.neo.2020.09.001. PubMed PMID: 32992138; PubMed Central PMCID: PMCPMC7522441.
43. Levine AJ. p53: 800 million years of evolution and 40 years of discovery. Nature reviews Cancer. 2020;20(8):471–80. Epub 2020/05/15. doi: 10.1038/s41568-020-0262-1. PubMed PMID: 32404993.
44. Gaumer S, Guénal I, Brun S, Théodore L, Mignotte B. Bcl-2 and Bax mammalian regulators of apoptosis are functional in Drosophila. Cell death and differentiation. 2000;7(9):804–14. Epub 2000/10/24. doi: 10.1038/sj.cdd.4400714. PubMed PMID: 11042675.
45. Moriishi T, Fukuyama R, Miyazaki T, Furuichi T, Ito M, Komori T. Overexpression of BCLXL in Osteoblasts Inhibits Osteoblast Apoptosis and Increases Bone Volume and Strength. J Bone Miner Res. 2016;31(7):1366–80. Epub 2016/02/09. doi: 10.1002/jbmr.2808. PubMed PMID: 26852895.
46. Funk K, Czauderna C, Klesse R, Becker D, Hajduk J, Oelgeklaus A, et al. BAX Redistribution Induces Apoptosis Resistance and Selective Stress Sensitivity in Human HCC. Cancers. 2020;12(6). Epub 2020/06/04. doi: 10.3390/cancers12061437. PubMed PMID: 32486514; PubMed Central PMCID: PMCPMC7352885.
47. Gohel A, McCarthy MB, Gronowicz G. Estrogen prevents glucocorticoid-induced apoptosis in osteoblasts in vivo and in vitro. Endocrinology. 1999;140(11):5339–47. Epub 1999/10/28. doi:

10.1210/endo.140.11.7135. PubMed PMID: 10537165.

Figures

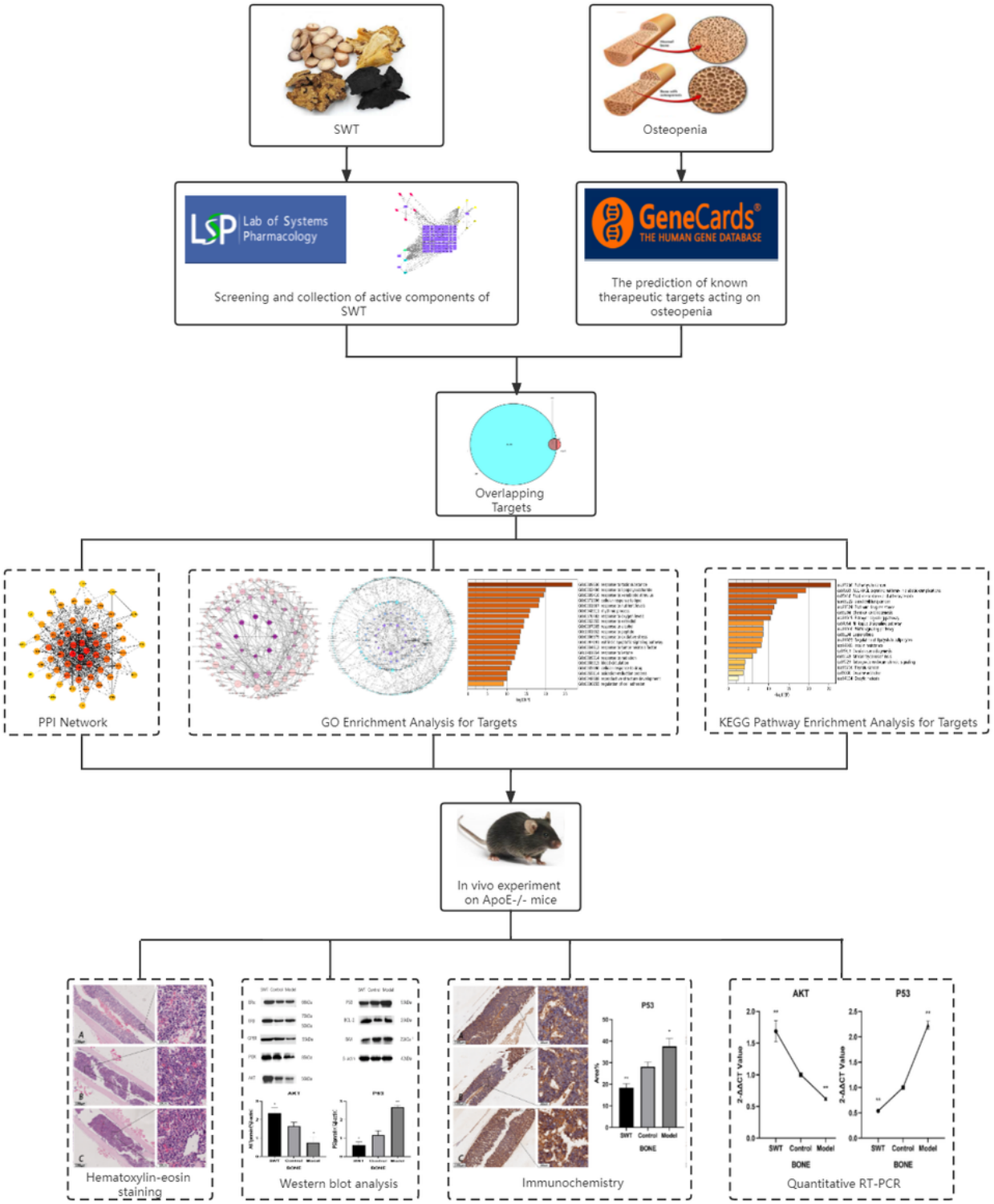

Figure 1

The flowchart of network pharmacology-based strategy for deciphering the mechanisms of SWT acting on osteopenia.

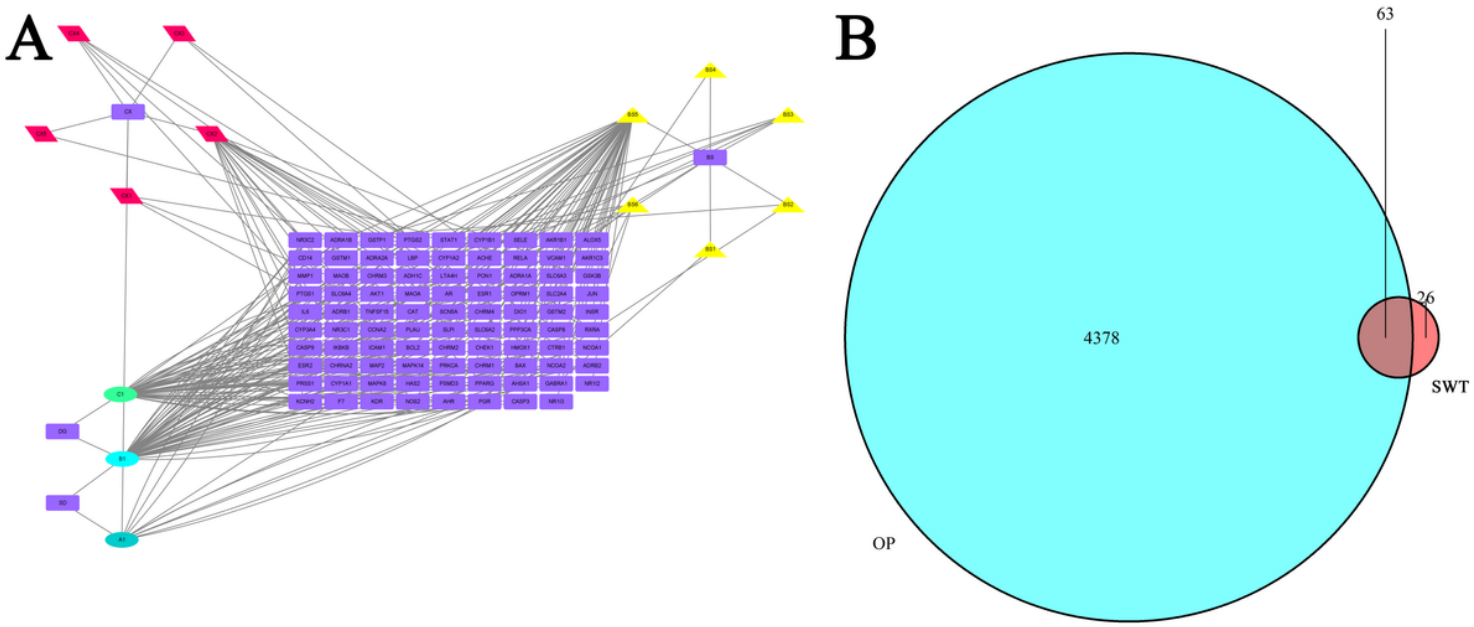

Figure 2

Prediction of compound-related targets and osteopenia -related targets. (**A**) active components of SWT. (**B**) Venn diagram of SWT treating on osteopenia.

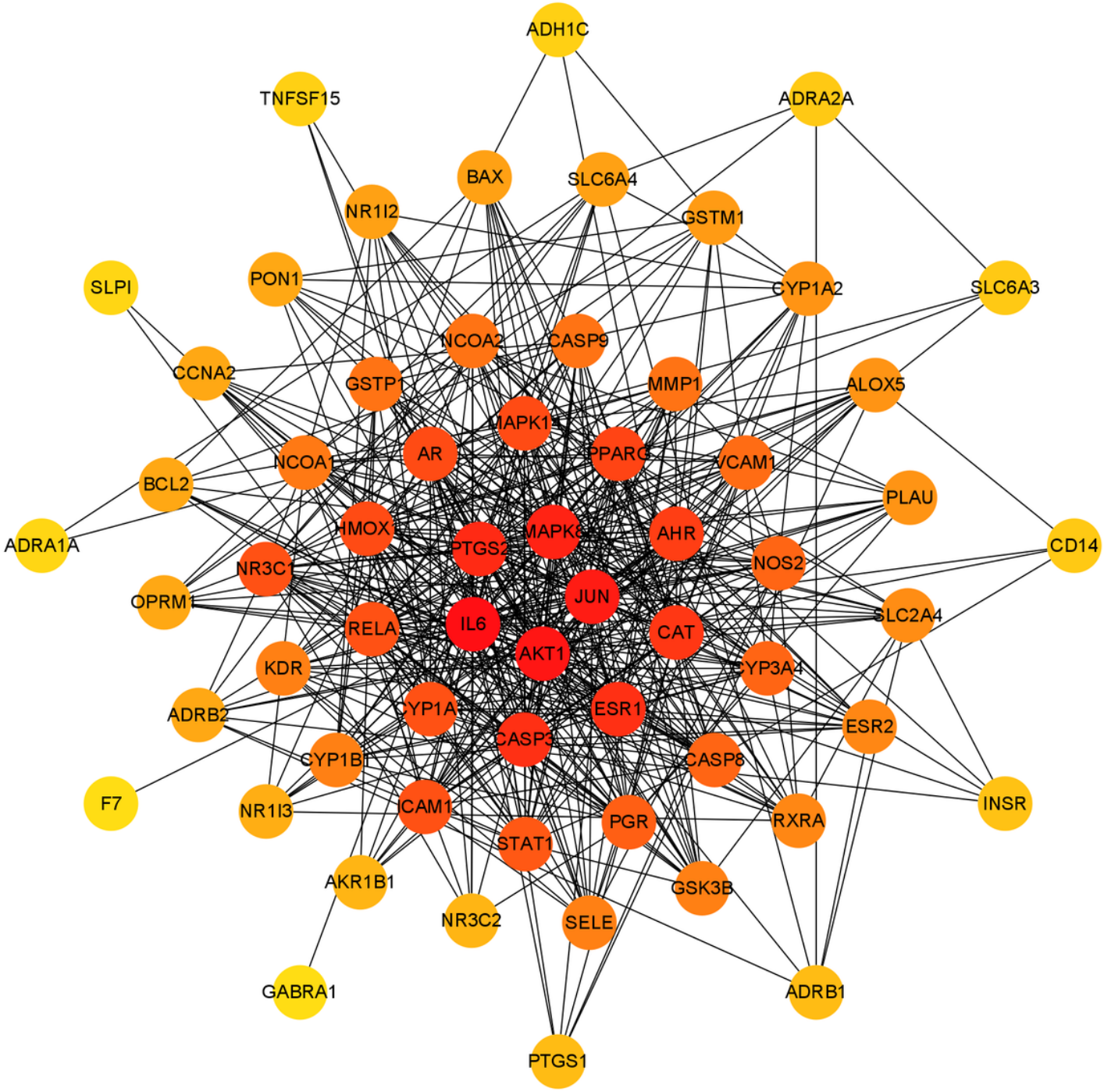

Figure 3

Protein–protein interaction (PPI) network of targets of SWT against osteopenia.

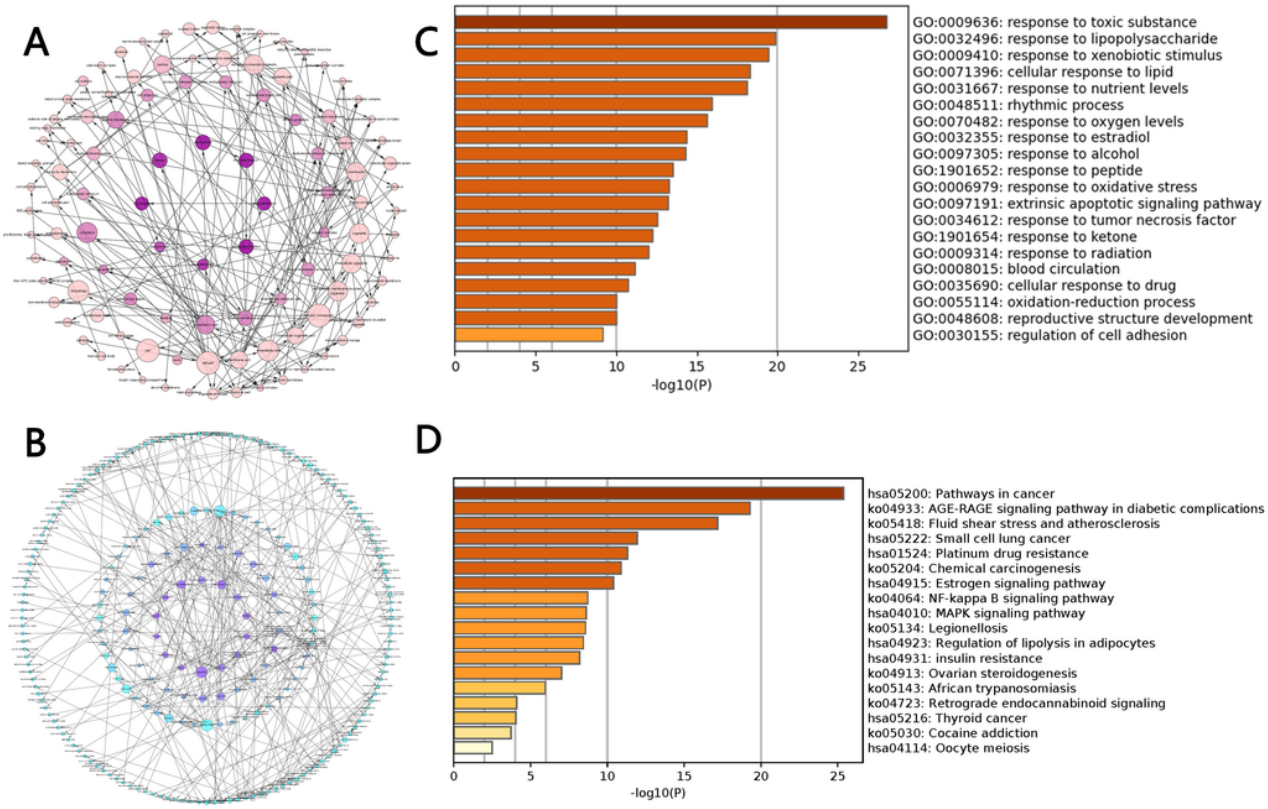

Figure 4

Biological process and pathway enrichment analysis. (**A, B and C)** GO enrichment analysis (Cellular component, Molecular functions and Biological process) for potential targets of SWT-osteopenia. (**D)** KEGG pathway enrichment analysis for potential targets of SWT-osteopenia. (*q* value refers to -log10 *P* value)

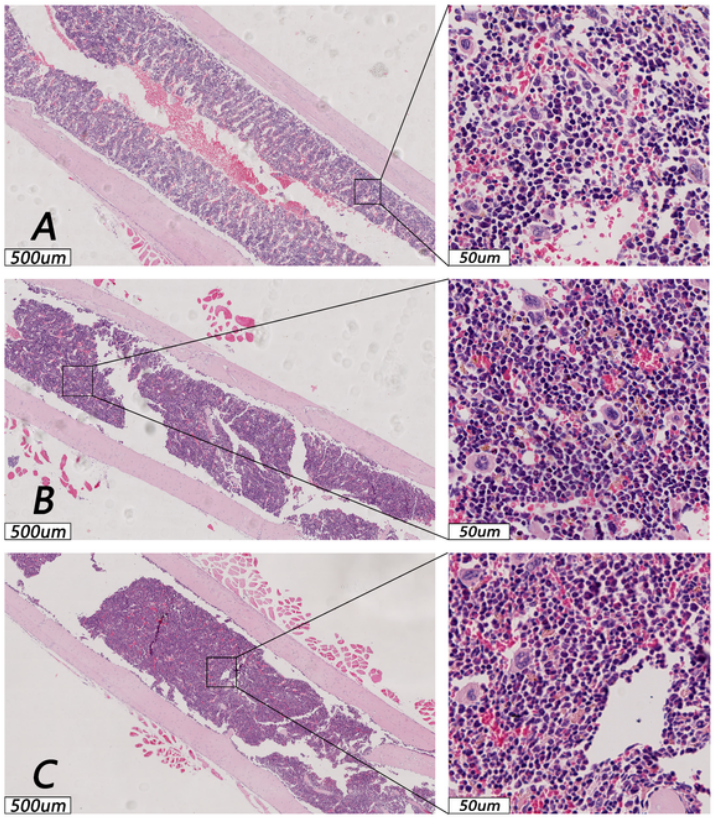

Figure 5

HE staining to observe the pathological tissue morphology of mice

Note: A: SWT group, B: Control group, C: Model group.

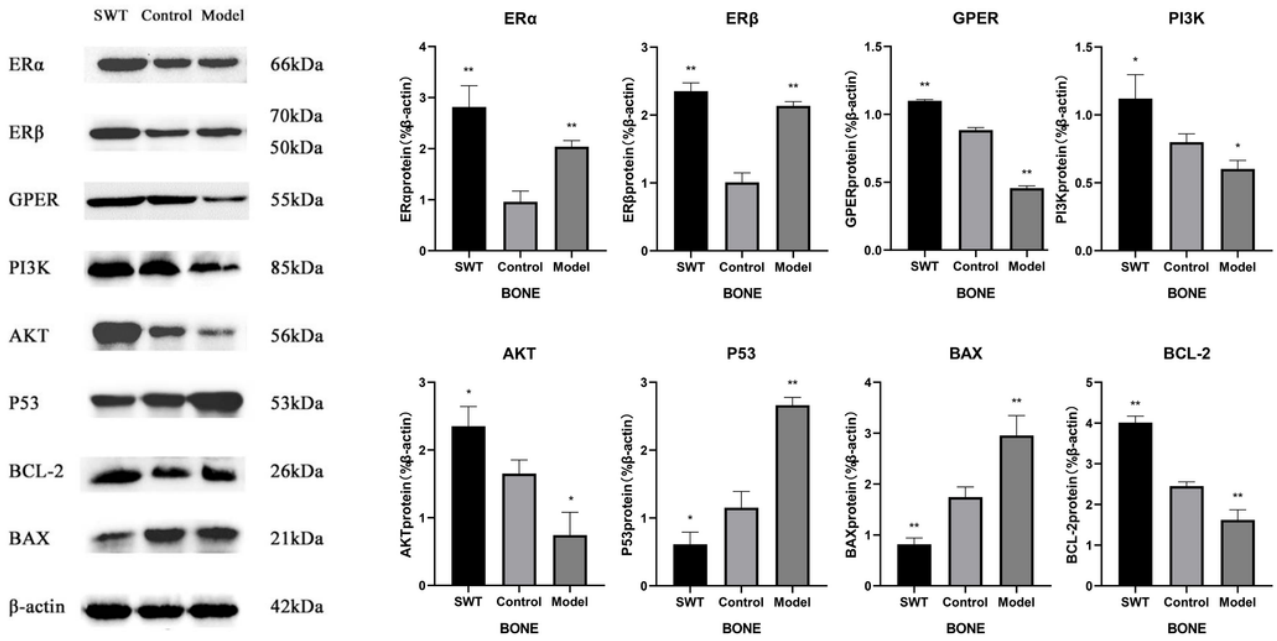

Figure 6

Western blot analysis was used to detect the expression level of proteins. a,b WB charts of the expression level of ERα, ERβ, GPER, PI3K, AKT, P53, BCL-2 and BAX in the femoral tissue of each group of mice.

Note: A SWT group, B: Control group, C: Model group.

Compared with the Control group, *$p < 0.05$, **$p < 0.01$

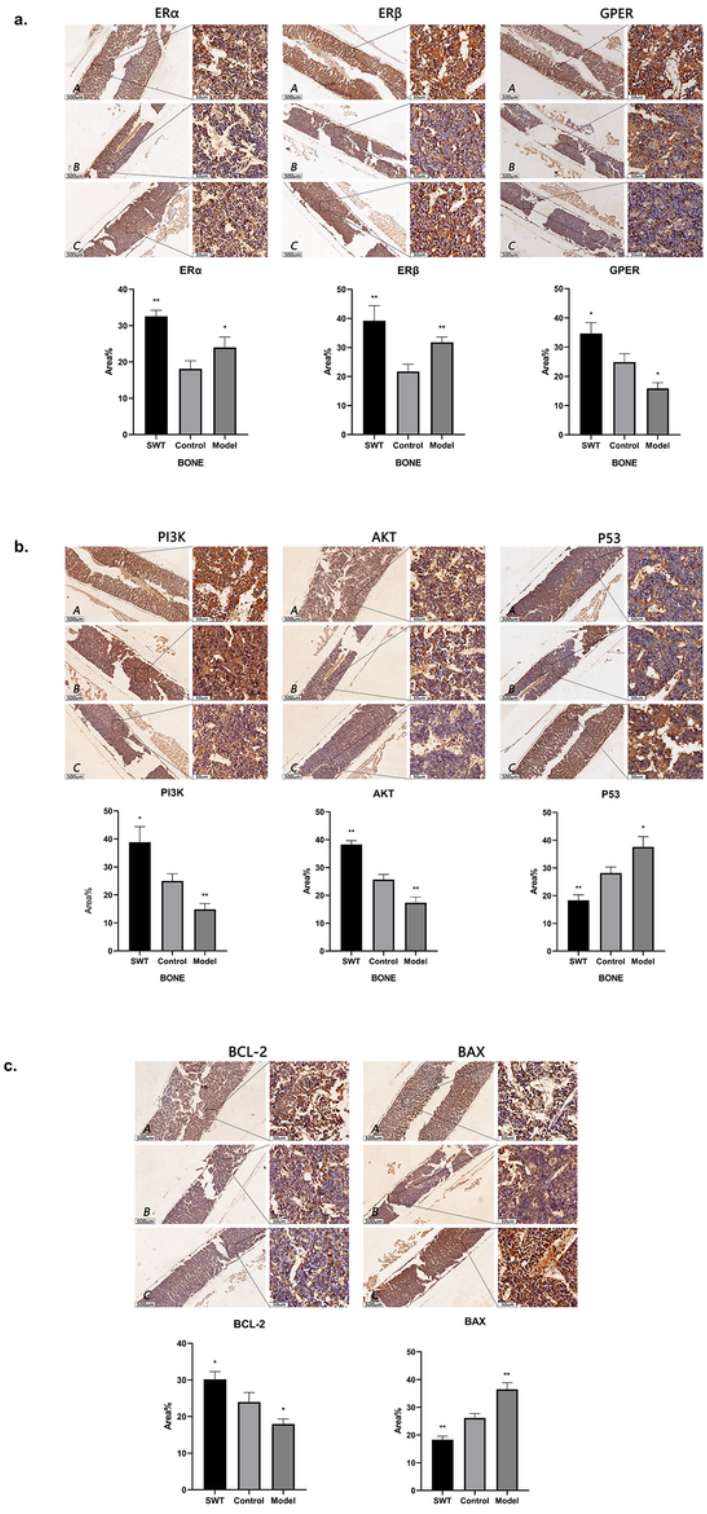

Figure 7

Immunohistochemical analysis to detect the expression position and expression level of the proteins. (A) The expression levels of receptor protein, including ERα, ERβ, GPER. (B) The expression levels of PI3K, AKT, P53. (C) The expression levels of BCL-2 and BAX.

Note: In each part, A. SWT group, B. control group, C. model group.

Compared with the blank group, *$p < 0.05$, **$p < 0.01$

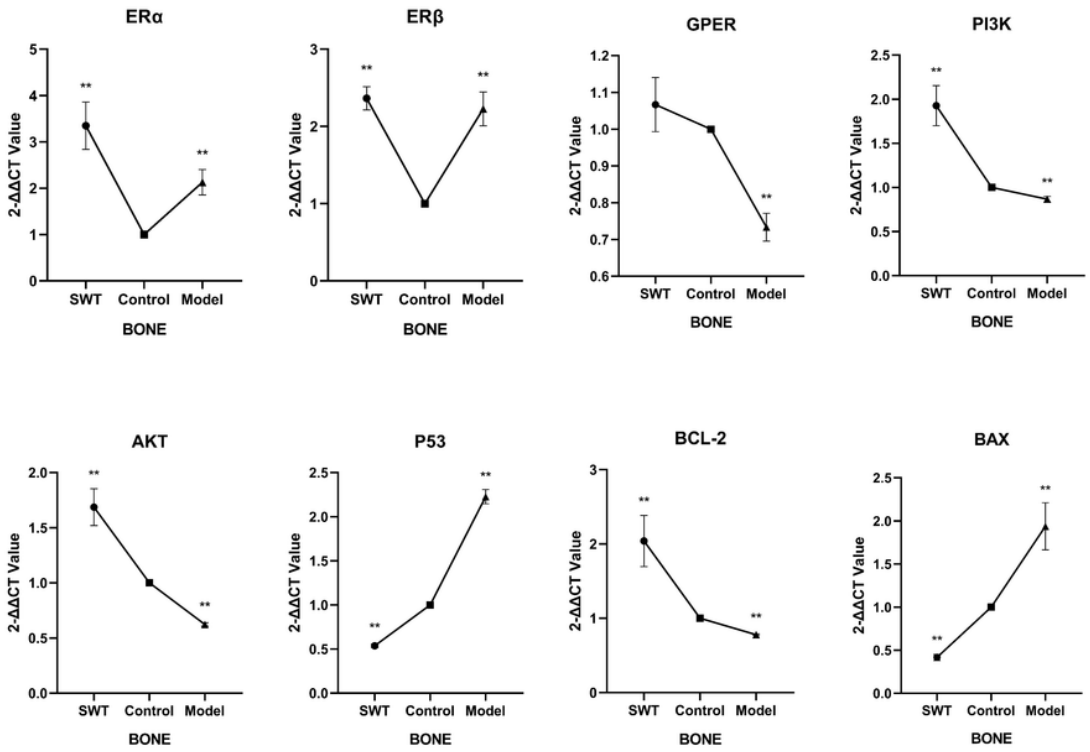

Figure 8

RT–PCR was used to detect the mRNA expression level of ERα, ERβ, GPER, PI3K, AKT, P53, BCL-2 and BAX in the femoral tissue of each group.

Note: SWT: Si-Wu-Tang group, Control: control group, Model: model group.

Compared with the control group, *$p < 0.05$, **$p < 0.01$

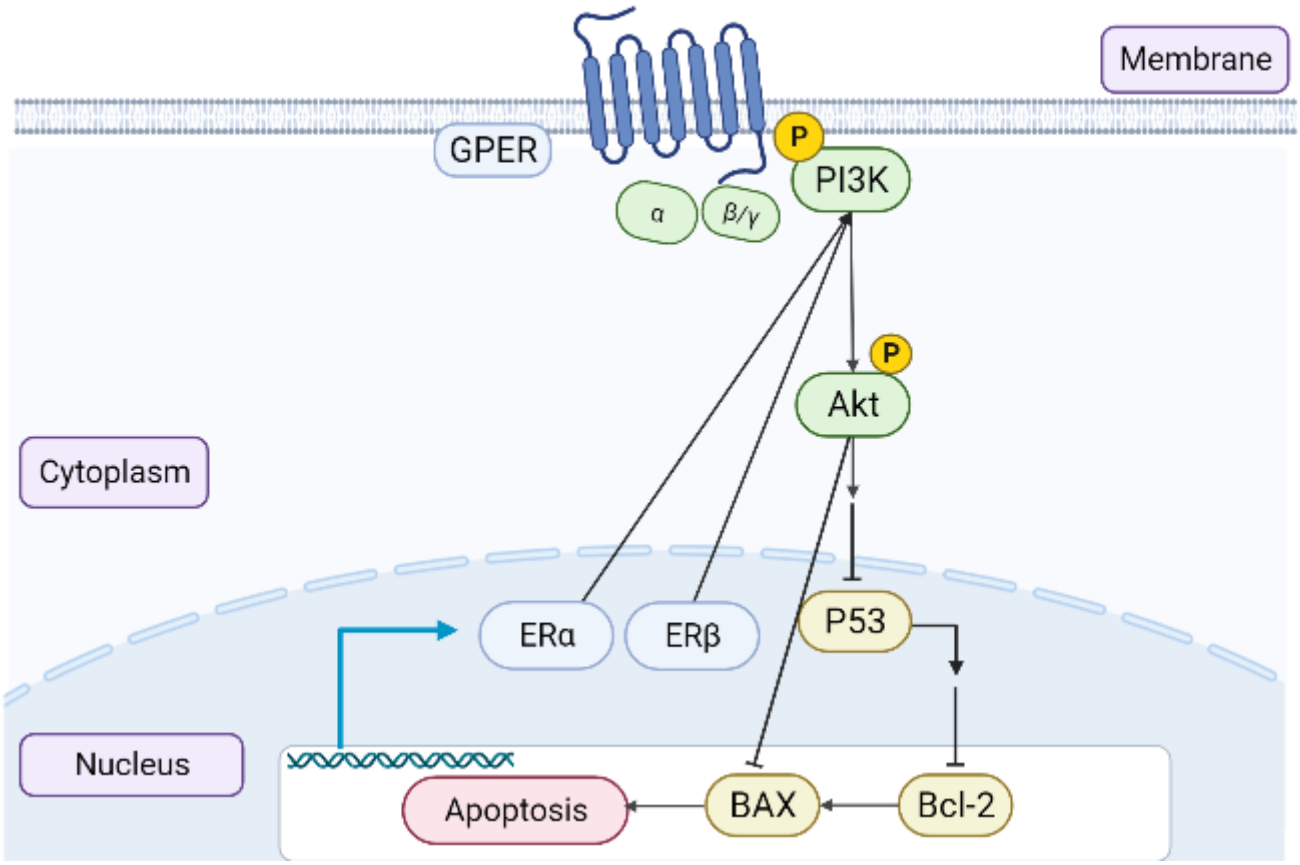

Figure 9

Estrogen signaling pathway.

Supplementary Files

This is a list of supplementary files associated with this preprint. Click to download.

- SupplementaryFig.1docx.docx
- Supplementarytable1.docx